Int. J. Electrochem. Sci., 17 **(2022)** Article Number: 221128, doi: 10.20964/2022.11.07

International Journal of
ELECTROCHEMICAL
SCIENCE
www.electrochemsci.org

State of Health Estimation Based on GAN-LSTM-TL for Lithium-ion Batteries

Guangyi Yang[1], *Qianhui Ma*[2,*], *Hao Sun*[3], *Xiaoyu Zhang*[3]

[1] Engineering Research Center, Ministry of Education of Automotive Electronics Drive Control and System Integration, Harbin University of Science & Technology, Harbin, China
[2] School of Electrical and Electronic Engineering, Harbin University of Science & Technology, Harbin, China
[3] The College of Artificial Intelligence, Nankai University, Tianjin, China
[*]E-mail: ma_qianhui0407@163.com

Received: 5 July 2022 / *Accepted:* 30 August 2022 / *Published:* 10 October 2022

The state of health (SOH) is a critical parameter for characterizing the current state of a lithium-ion battery. In recent years, SOH estimation methods that employ machine learning and deep learning have invariably been the research hotspots for researchers in recent years. In the previous work paper, a battery SOH online estimation method based on GAN-LSTM algorithm was proposed to overcome the defects such as a large amount of computation and long-time consumption for prediction and to find a prediction method suitable for the time series data characteristics of lithium-ion batteries. Among the work, generative adversarial networks (GAN) are used to process the corresponding feature data and 30% of the dataset is selected to generate the dataset used for training. A long short-term memory (LSTM) network is used to learn the mapping relations between features and SOH. Transfer learning (TL) is utilized to enhance the adaptability of the LSTM network and achieve accurate SOH estimation by solving training and test problems between datasets of various lithium-ion batteries. The NASA battery sample dataset and the battery cycle aging test experimental dataset of the Advanced Life Cycle Engineering Center of the University of Maryland are used for experimental verification. The analysis of experimental results demonstrates that the model boasts pinpoint accuracy and incredible adaptability across multiple datasets.

Keywords: Lithium-ion battery, State-of-Health (SOH), Long short-term memory (LSTM), Generative adversarial networks (GAN), Transfer learning (TL).

1. INTRODUCTION

With ongoing economic expansion, environmental degradation has become increasingly problematic in latest days, and fossil reserves have progressively depleted. Compared with conventional fuel vehicles, electric vehicles have drawn attention due to their efficacy in lowering oil demand and gas

emissions while boosting energy conversion efficiency [1]. At the moment, the durability and safety of lithium-ion batteries have turned into significant impediments to the development of electric vehicles. As operating duration increases, battery performance degrades gradually, resulting in problems such as decreased capacity, greater resistance, and increasing cell inconsistency [2]. The SOH of the battery is one of the most crucial monitoring contents in the operation of the battery. Accurate estimation of SOH can not only determine the present health state of the battery, but also anticipate its service life and assure its safe operation [2].

Common SOH estimation methods mainly include experimental measurement or analysis methods, model-based methods and data-driven methods. In the first method, the direct measurement method typically involves a capacity test method, an internal impedance-based method, an open-circuit voltage (OCV) method and a coulomb-counting method [3]. The OCV method, which calculates capacity based on the relationship between SOC and OCV, requires a long rest period to obtain a steady battery condition in order to estimate SOH. SOH is obtained by integrating the current during the entire operating process, which consumes a lengthy time [4]. In addition, the internal impedance-based method [5] is an accurate measurement technique that measures battery impedance under a variety of temperature and SOC conditions, but is susceptible to laboratory temperature. In comparison to the direct method, the indirect analysis method estimates SOH by measuring some feature parameters that can reflect battery degraded capacity, such as electrochemical impedance spectroscopy (EIS) analysis, voltage trajectory analysis, capacity increment analysis and harmonic analysis of battery nonlinear characteristics [6], all of which are commonly limited by measurement equipment.

The model-based method is a widely used method, which is mainly divided into electrochemical model method, equivalent circuit model method and filter-based method. The electrochemical model method uses the battery equivalent model to design the system, and uses the battery capacity obtained by online monitoring to estimate the SOH [7]. The equivalent circuit model method uses relatively basic electrical components to build an equivalent circuit model of the battery which is combined with a large amount of data to analyze the SOH. Commonly used models include RC model, Rint model and Thevenin model. Filter-based methods are also called indirect method which combine filters (such as Kalman filter or particle filter) to estimate SOH based on SOC and OCV. Among them, the Kalman filter (KF) uses a recursive method to compare the previous estimated value with the current measured value to reduce the error and thus improve the estimation accuracy [8]. The problem with this approach is that traditional Kalman filters are not suitable for nonlinear battery models. To solve this problem, XI A et.al proposed a SOH estimation method based on nonparametric aging model and particle filter [9]. And Rossi, C et.al proposed an extended Kalman filter (EKF) method to estimate SOH and SOC based on battery surface temperature changes [10]. Xu et al. [11] introduced a framework based on unscented Kalman filtering (UKF) based on the electrochemical model for simulating battery charge and discharge, which achieved higher accuracy in the prediction of RUL. However, the performance of these methods is highly dependent on the accuracy and robustness of established battery models or observers. Also, since the state equation and model parameters are defined by the battery used, and the battery parameter values change over time during the charging and discharging process, so these factors will increase the error of the estimation [12].

The date-driven method is based on samples from the original battery test data, and obtains the variation rules of battery performance during battery aging via a specific mechanism, so as to estimate the SOH relying on these rules. This method is appreciated for its flexibility and effectiveness in indirect observability. Numerous data-driven methods exist, namely machine learning, regression algorithms, and support vector machine algorithms. Jo et al. [13] investigates several machine learning strategies for training and enhancing SOH prediction of fresh battery aging cycles using a dataset of LIB degradation curves. Zhou et al. [14] proposes an innovative loop synchronization method that uses dynamic time warping (DTW) to change the existing coordinate system to achieve isometric inputs to the estimated model while preserving all information. Li et al. [15] uses the ensemble learning AdaBoost model to integrate the PSO-SVM regression model, and constructs a strong regressor by merging multiple weak learners, strengthening the stability of lithium-ion battery health state prediction. However, the lithium-ion battery data is time-series correlation, and the amount of data is vast, requiring the model to possess high prediction accuracy. As a result of its specific memory ability and capacity to process time series data, LSTM has garnered a substantial amount of attention. Zhang et al. [16] proposed an online SOH estimation method for LIB method that combines LSTM with an attention mechanism (AM). The LSTM neural network is used to learn the mapping relationship between the parameters, and then AM is used to select the relevant hidden states of the LSTM across all time steps, resulting in distinct weights for each hidden state, thereby solving the problem of detailed state information extraction. Liu et al. [17] exploited the connection between dQ/dV and SOH to fit diverse black box models through LSTM network, and designed an online swift and accurate estimation method based on the fusion of the advanced ICA method and LSTM neural network. Nonetheless, as research has proceeded, further attention has been drawn to the difficulties that occur in the SOH prediction of lithium-ion batteries based on LSTM: the first is how to properly process the original data to improve the accuracy of the prediction, and the second is how to solve the prediction process The third is how to reduce the workload of SOH estimation for different types of batteries.

In order to better manage the data set required by LSTM and improve the accuracy of prediction, different machine learning methods are used to optimize the model. GAN is extensively adopted among them due to its benefits in data production and processing. Wang et al. [18] used GAN to alleviate the problem of data imbalance, and by lowering the quantity of original data, it may eliminate the possible overfitting concern and promote prediction accuracy. Pushpak et al. [19] constructed a network model based on PAC-LSTM-GAN on the basis of LSTM, which effectively bridged the gap between each dataset and improved the reliability of model operation. Javaid et al. [20] integrated machine learning methods such as GAN, CNN and ERNET, and extremely facilitated the performance indicators of all aspects of the model based on the LSTM model.

There are numerous sorts of lithium-ion batteries, and the datasets vary in size and format. Transfer learning (TL) is increasingly being used to make the same model applicable to diverse battery datasets and meet the goal of reducing burden. Li et al. [21] introduced deep transfer learning to accelerate the model training process and developed state estimators with multiple forms of battery data. Bao et al. [22] conducts trials on several datasets, which enhances the robustness and generalization ability of the model.

In summary, we propose a GAN-LSTM-TL-based SOH estimation method for Lithium-ion batteries. Processing and normalizing a large amount of data through the improved GAN network improves prediction accuracy while decreasing training time. Afterwards, using the processed data to train the LSTM network not only exploits the advantages of LSTM in processing time series data, but also prevents challenges like vanishing gradients as well as exploding gradients. Finally, the TL (transfer learning) method is used to apply the trained model to other datasets, which reduces the workload and training time and enhances the generalization capability of the model. In the simulation experiments, we applied the designed models to the NASA battery sample data set of the National Aeronautics and Space Administration and the battery cycle aging test experimental data set of the Advanced Life Cycle Engineering Center of the University of Maryland in the United States. Get higher SOH prediction accuracy.

The remainder of this thesis is structured as follows: Section II discusses the aging process of Li-ion battery SOH and introduces the adopted dataset; Section III explains the GAN, LSTM and TL algorithms used in this study; Section IV It is the analysis of the experimental results of this thesis; and Section V concludes this thesis.

2. LITHIUM-ION BATTERY AGING PROCESS

In this section, the aging process of lithium-ion batteries used in the NASA battery cycle aging test experiment is analyzed. The resultant datasets were selected to be processed and calculated to get the Pearson coefficient which can be used to verify the effectiveness of feature parameter processing.

2.1. Definition of SOH

The SOH value of a lithium-ion battery is an important indicator to quantify the battery health, which can reflect the aging state of the battery and predict the battery life. The SOH is defined by battery capacity which is the most widely used representation and the predictive expression of SOH is as follows:

$$SOH = \frac{C_{aged}}{C_{new}} \times 100\% \qquad (1)$$

Among them, $Cnew$ is the rated capacity of the lithium-ion battery, and $Caged$ is the current capacity of the lithium-ion battery. The SOH value of a new battery is 100%, and the SOH value will continue to decrease while the battery being used. It is generally believed that the life of a lithium-ion battery ends when the SOH drops to 80%.

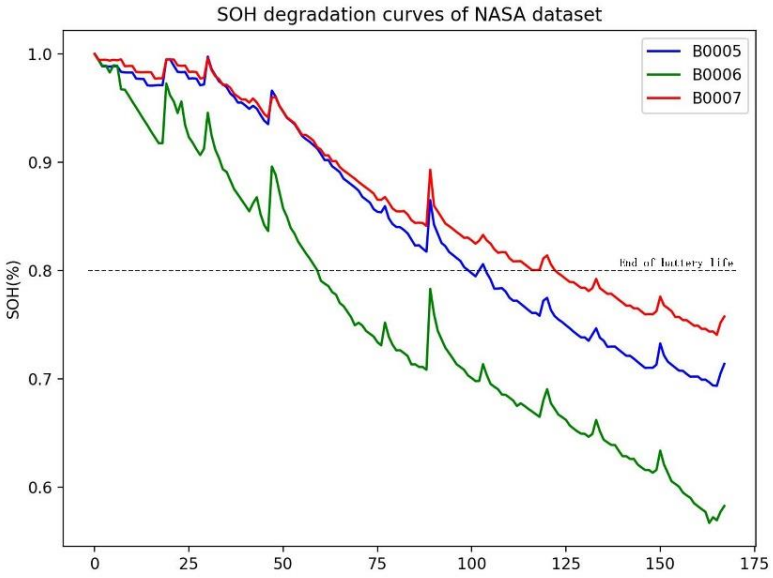

Figure 1. The SOH curves of NASA's batteries

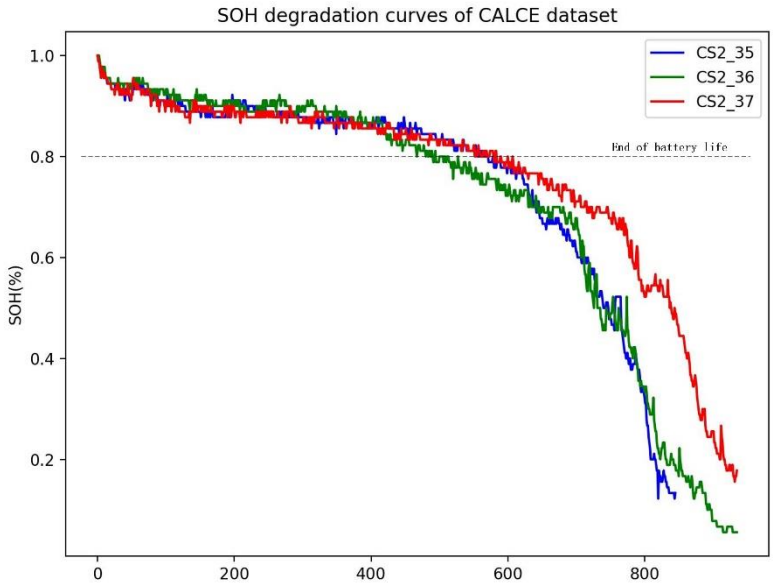

Figure 2. The SOH curves of CALCE batteries

2.2 Datasets

Two datasets were used in this study, one is from the NASA Ames Prognostics Center of Excellence and the other is from the Center for Advanced Life Cycle Engineering (CALCE) at the University of Maryland.

(1) The selected samples from the datasets provided by NASA Research Center were B5, B6, B7, and B18 batteries with a rated capacity of 2Ah. The test experiments were carried out at room temperature of 24℃, and all the batteries were charged and discharged using the same standard constant

current/voltage. First, the constant charging current rate was kept at 0.5 C until the voltage reached 4.2V, then the constant voltage charging was maintained, and the voltage was maintained at 4.2V until the charging current was lower than 0.05 A. After that, keep the 2A constant current discharge until the voltage dropped to 2.7V, 2.5V, 2.2V, and 2.5V, respectively. The experiment ended when the battery reached the end of its life and the rated capacity degraded from 2Ah to 1.4Ah. For more details of the experimental process and data characteristics, please refer to [23].

The SOH curves of selected NASA batteries are shown in Figure 1.

(2) The sample selected from CALCE datasets is CS2 battery. The test experiment was carried out at room temperature. All the batteries used the same standard constant current/voltage charging and discharging method. First keep the constant charging current rate at 0.5 C until the voltage reached 4.2V, then keep the constant voltage charging at 4.2V until the charging current was lower than 0.05 A. Unless otherwise indicated, the discharge cut-off voltage is 2.7V.

All batteries were randomly numbered and cycled multiple times under corresponding conditions. The name 'CS2_n' is the nth numbered cell and the data file for each cell contains a set of log data tables generated by the test. All the batteries were tested using an Arbin battery tester. See [24] and [25] for specific experimental procedures and data characteristics.

The SOH curves of CALCE batteries are shown in Figure 2.

2.3 Feature selection

The SOH feature parameters of lithium-ion batteries roughly include internal resistance, cycle times, capacity, temperature and charging, discharging voltage, current, and time. The internal resistance is related to SOC and temperature, which is not easy to measure. The remaining cycle times and total cycle times are of bad maneuverability and cannot be accurately used to predict the SOH. Beside, the voltage is not suitable for the experimental method of the data set used. The capacity is the external performance of the battery, which can be obtained by calculating the current and the charging and discharging time. Its comprehensiveness is stronger than other features. It is convenient to measure the charging and discharging time And the aging of the battery can be evaluated intuitively. In addition, the temperature is an important factor when the battery is working, which can reflect the health and working conditions of the battery . And it is easier to be obtained than other features. It can be seen that with the increase of battery aging, the battery capacity will gradually decrease, and the charging and discharging time will also gradually shorten. In addition, during the measurement process, the battery temperature fluctuated and increased, while the peak value of the charging current showed a clear downward trend. Therefore, some features such as capacity, charging and discharging time, and temperature were used. By the way, the aging characteristics are extracted by comprehensively considering the peak value of the charging current.. The specific relationship between the battery SOH and the charging and discharging time and temperature is shown in Figure 3.

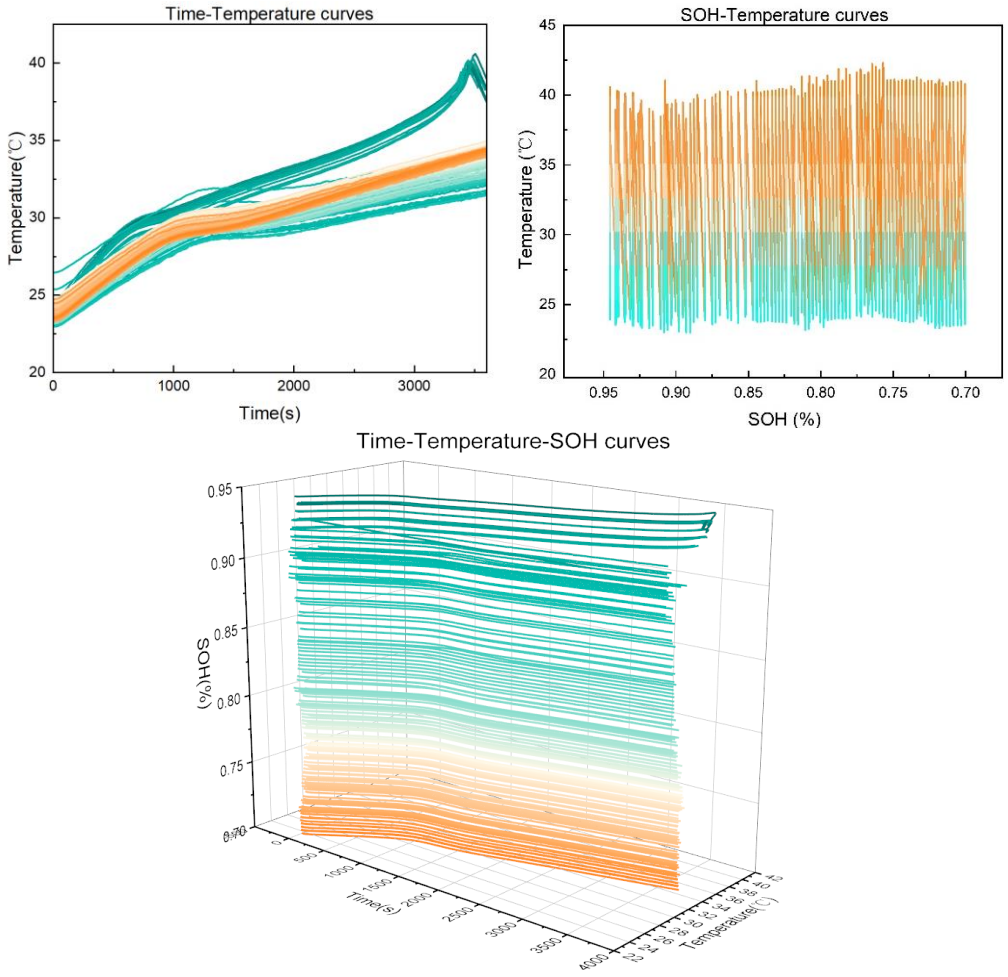

Figure 3. The curves of SOH-time-temperature

It can be seen from Figure 3 that the temperature of the battery increases cyclically as the number of cycles increases over time. In each cycle, the SOH value drops significantly. The reason is, in the process of constant current charging of the battery, the discharge cut-off voltage decreases, resulting in an increase in the internal resistance of the battery, which makes heat generation and an increase in temperature, and the aging of the battery is accelerated, which results in a significant decrease in the SOH of battery. At the end of charge and discharge, the current decreases, and the heat generated also decreases, resulting in a drop in temperature, and the degree of SOH drop will also slow down.

3. METHODOLOGY

In this section, a novel SOH estimation method is proposed based on GAN-LSTM-TL. Firstly, the optimized GAN is used to process the corresponding large amount of feature dataset for training. Next, the LSTM is combined with the FC layer to build the basic model and train the model with the data generated by the GAN to obtain the SOH estimation result. Finally, a transfer learning method is

adopted to improve the adaptability of the model and achieve accurate SOH estimation for different battery datasets.

3.1. Generative Adversarial Networks

Generative Adversarial Networks, proposed by Ian Goodfellow et al., is a currently popular deep neural network for training generative models by reducing complex calculations that approximate many probabilities [26]. GAN is composed of generator G(·)and discriminator D(·), and its model structure is shown in Figure 4. The generator G(·) takes a uniform noise vector z as input and gets the generated data G(z). The discriminator D(·) needs to determine as much as possible whether the input data is the real x or the G(z) generated by the generator. In this way, the generator and discriminator continuously optimize and adjust their own parameters in the process of adversarial training, and finally make the generator generate data that tends to the real value [27].

The objective function V(D,G) of the GAN model is as follows:

$$V(D,G) = E_{x\sim P_{data}}[logD(x)] + E_{x\sim P_z}\{\log\{1 - D[G(z)]\}\} \qquad (2)$$

Among them, z obeys the prior distribution P, x obeys the real lithium battery data distribution $Pdata$, $E(\cdot)$ is the calculation of the expected value, $D(\cdot)$ is the probability that the discriminator judges that x is the real data, and $D[G(z)\ ]$ is the probability that the discriminator judges that $G(z)$ is the real data. When training the generator G, it makes $D[G(z)]$ approach 1 as close as possible and minimizes the objective function. When training the discriminator D, it makes $D[G(z)]$ approach 0 as close as possible, making $D(x)$ approach 1 and maximizing the objective function.

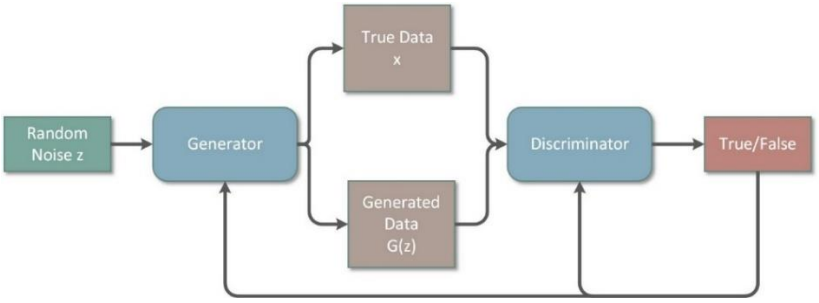

Figure 4. Structure diagram of GAN model

3.2. Long Short-Term Memory Network

To deal with time series data, a neural network with a recurrent structure called Recurrent Neural Networks (RNN) has been proposed. With the virtue of the neurons that are interactively connected between layers, RNN can not only process the previous input information but also memorize the previous information. However, as the memory for long input sequences is shortened, the problem of vanishing

and exploding gradients may occur [28]. Therefore, Long Short-Term Memory Network is designed to process longer time series data.

LSTM realizes the function of filtering redundant information by adding a complex gate structure. An LSTM network contains input gates for determining the input information, forget gates for forgetting information and output gates for controlling the output. The LSTM network selects whether to update and forget information through multiple logic control units composed of three kinds of logic gates, so as to overcome the problems that it is difficult for RNN to learn earlier information and the gradient disappears. The general LSTM network structure is shown in Figure 5.

The forward propagation process of the LSTM network is as follows:

(1) Forgetting gate

First, the LSTM network determines which data should be discarded by setting the forgetting gate, as shown below:

$$f_t = \sigma\left(W_f[h_{t-1}, x_t] + b_f\right) \qquad (3)$$

Among them, σ is the sigmoid function, which is used to activate the forget gate.

W_f—the weight coefficient of the linear relationship;

b_f—the weight offset of the linear relationship;

The forget gate will read the hidden layer h_{t-1} and the input x_t from the previous moment, and

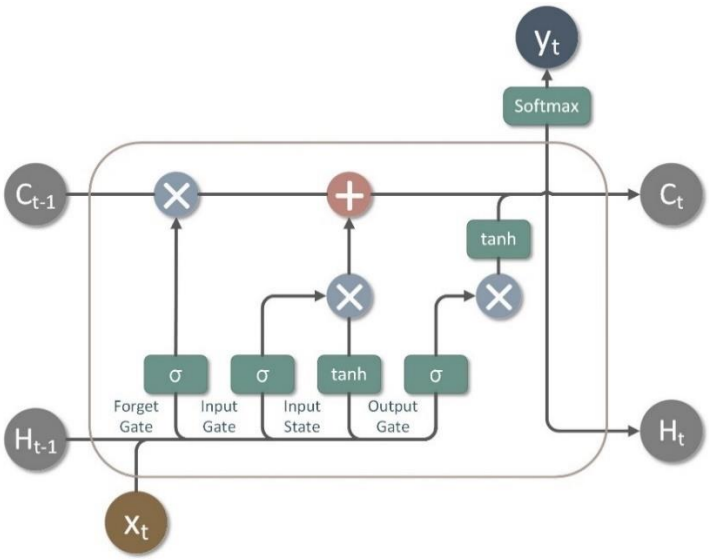

Figure 5. Network structure diagram of the LSTM

then put the value from 0 to 1 into the cell state. 0 means that the transmission data is completely abandoned, and 1 means that the data is completely saved.

(2) Input gate

The input gate is used to determine what kind of information to save, and make it pass through the σ activation function. Then it is cross-multiplied with the information passing through the tanh activation function to give the cell state a new $\widetilde{C_t}$ input as follows:

$$i_t = \sigma(W_i[h_{t-1}, X_t] + b_i) \quad (4)$$

$$\widetilde{C_t} = tanh(W_c[h_{t-1}, X_t] + b_c) \quad (5)$$

Among them, W_i and W_c are the weight matrices of the input gate, b_i and b_c are the input gate bias.

(3) Update the cell state

After the first two gates, the LSTM network has decided what information to retain and forget. Next, it needs to update the new information into the cell state and multiply the old cell state $\widetilde{C_t}$ by the forget gate f_t, so as to forget the information that needs to be discarded, and finally add the values of it and $\widetilde{C_t}$ to get the current state C_t. The updated cell state is as follows:

$$C_t = f_1 * C_{t-1} + i_t * \widetilde{C_t} \quad (6)$$

(4) Output gate

At the end of the network, the output gate is used to determine the desired output value. Pass the input through the σ activation function, and cross-multiply it with other information that passes through the $tanh$ activation function, and finally get the part that determines the output, as follows:

$$O_t = \sigma(W_o[h_{t-1}, X_t] + b_o) \quad (7)$$

$$h_t = O_t * tanh(C_t) \quad (8)$$

Among them: σ——sigmoid activation function;

$tanh$——bitangent activation function;

f_t, i_t, O_t, C_t——forgetting gate, input gate, cell state and output gate at time t.

This thesis uses the Adam optimization method [29] to update the network weights and bias terms:

$$m_\varepsilon = \beta_1 m_{\varepsilon-1} \nabla L(W_{\varepsilon-1}) \quad (9)$$

$$\gamma_\varepsilon = \beta_2 \gamma_{\varepsilon-1} \nabla L(W_{\varepsilon-1})^2 \quad (10)$$

$$\widetilde{m_\varepsilon} = \frac{m_\varepsilon}{(1-\beta_1^\varepsilon)} \quad (11)$$

$$\widetilde{\gamma_\varepsilon} = \frac{\gamma_\varepsilon}{(1-\beta_2^\varepsilon)} \quad (12)$$

$$W_\varepsilon = \frac{W_{\varepsilon-1} - \alpha\widetilde{m_\varepsilon}}{(\widetilde{\gamma_\varepsilon} - \theta)} \qquad (13)$$

In the above formula:

m_ε, γ_ε——the decay factor of the initial L1 and L2 regularized decay matrices at the εth time;

$\widetilde{m_\varepsilon}$, $\widetilde{\gamma_\varepsilon}$——the updated matrices of $m\varepsilon$, $\gamma\varepsilon$;

β_1, β_2——the decay factor;

α——learning rate;

θ——constant, $\theta = \theta = 1 \times 10^{-8}$.

The model training will end when the number of iterations reaches the set value. After saving the trained model, perform training will multiple many times, and select the model with the best fitting effect for prediction.

3.2. Li-ion battery SOH estimation method based on GAN-LSTM-TL

Existing machine learning methods usually require large amounts of labeled data to train models. However, in practical applications, the limited sample size in the target domain often affects the experimental results. In order to transfer the knowledge and skills learned from the source domain to a new domain, and achieve the purpose of training a more accurate model with less data, a TL based on deep neural network has been proposed, which has attracted extensive attention [30].

As an efficient data mining framework, TL can transfer all or part of the features of the source domain to facilitate the model construction of the target domain, thereby avoiding "training from scratch" to learn new tasks. It can also be used to learn new tasks through the source domain information. The methods exploited by the target domain reduce the reliance on large amounts of data for training [31]. According to different transfer learning logics, TL can be divided into four categories: model-based, instance-based, feature-based, and relation-based. Among all TL schemes currently, fine-tuning of pre-trained models based on new datasets is the most popular way of learning in the field of machine learning [32]. The overall process is shown in Figure 6.

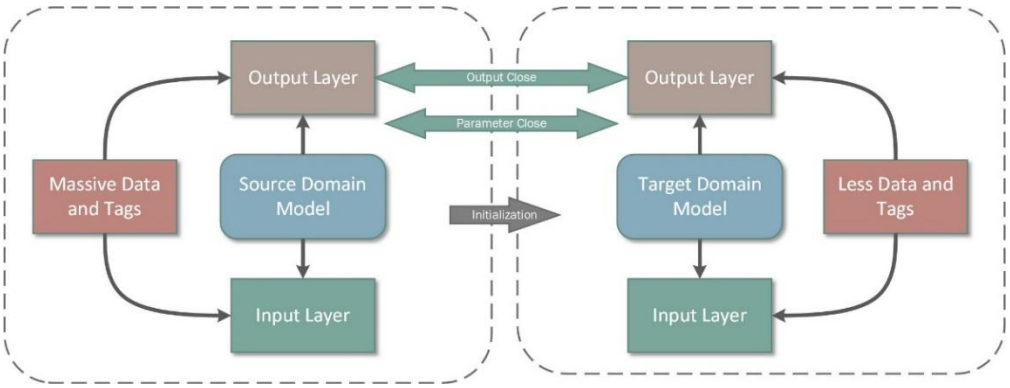

Figure 6. Structure diagram of Transfer Learning

Therefore, in order to cope with the dual challenges of small training datasets and high pre-training accuracy requirements, TL is added to the GAN-LSTM network to estimate the SOH of lithium-ion batteries, thereby improving the generalization ability of the model.

In order to obtain more accurate SOH estimation results of lithium-ion batteries, we propose a method for SOH estimation of lithium-ion batteries based on GAN-LSTM-TL. In this method, GAN is used to process the corresponding feature data to generate a dataset for training; the LSTM network is used to learn the dependency between feature quantities and SOH to obtain SOH estimation results; TL is used to improve the adaptation of the network model ability to achieve accurate estimation of battery SOH for different datasets. Different from the traditional method, we use different models and different sizes of data sets to conduct comparative experiments to verify the effect of transfer learning, so as to improve the generalization ability of the model. The overall process is shown in Figure 7.

Appropriate training ratio is the key to improve the generalization performance of the base model. Too much training data may cause overfitting, and lead the model to over-learn the private properties of the source task, which will affect the effect of transfer learning [33]. Therefore, in the model training stage, we selected 30% of B0005 and B0006 sample data as the training set, processed them through GAN, and generated the training set of LSTM on this basis. Finally, the B0007 sample data was used as the test set to verify the model accuracy.

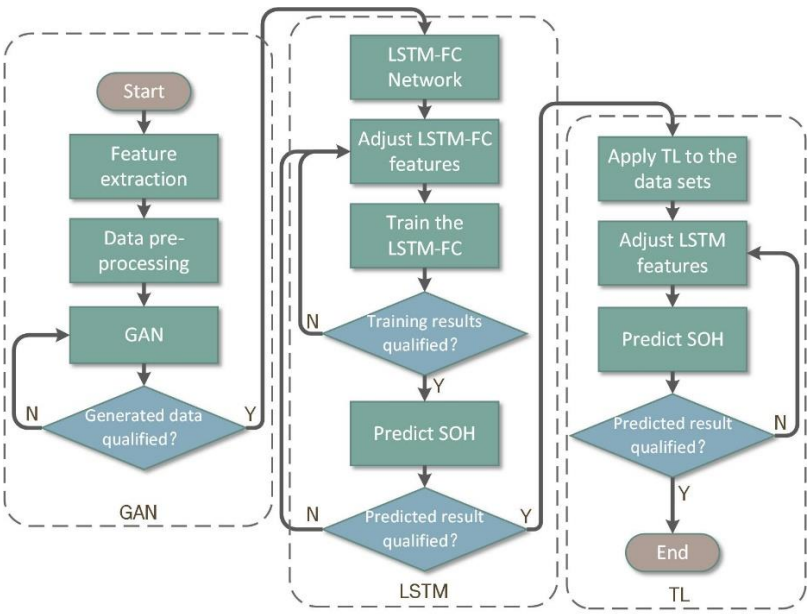

Figure 7. The flowchart of the proposed SOH prediction method based on GAN-LSTM-TL

4. EXPERIMENTAL RESULTS AND ANALYSIS

All experiments were run on a Lenovo Xiaoxin Pro 13IML computer equipped with Intel(R) Core(TM) i7-10710U CPU, 16G memory, 64-bit Windows 10 Home Chinese version, and the prediction

model was IDLE (3.10) in Python (version-3.10).) based on the Keras deep learning framework in the developing environment.

The prediction evaluation indicators include root mean square error RMSE (Root Mean Square Error) and mean absolute error MAE (Mean Absolute Error), etc. The calculation formula is as follows:

$$RMSE = \sqrt{\frac{\sum_{i=1}^{n}(\hat{y}_i - y_i)^2}{n}} \quad (14)$$

$$MAE = \frac{\sum_{i=1}^{n}|\hat{y}_i - y_i|}{n} \quad (15)$$

In the above formula:

y_i——Original data result;

$\hat{y}_i$——Predicted result;

n——Battery cycle period.

4.1. Performance of GAN-LSTM on NASA dataset

First, we use the first 20% of the B0007 dataset for training and the last 80% to verify the prediction effect of the GAN-LSTM model.

The parameters of the GAN neural network model are set as follows:

The number of GAN layers is 2, the sliding window size is 64, the number of samples (batch size) is 64, the learning rate is 0.001, and the maximum number of iterations is 30,000.

The parameters of the LSTM neural network model are set as follows:

The number of LSTM layers is 2, the sliding window size is 6, the number of samples (batch size) is 6, the learning rate is 0.01, the maximum number of iterations is 300, and the last layer is set as a fully connected layer. To enhance robustness, a Dropout layer with a value of 0.1 is also set.

The prediction results and error curves of the model are shown in Figure 8.

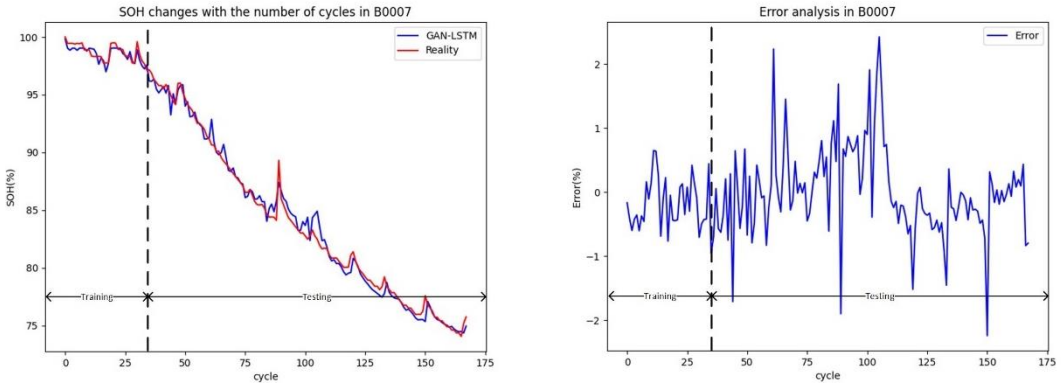

(a) SOH changes with the number of cycles (b) Error analysis

Figure 8. Performance comparison of GAN-LSTM on B0007 dataset.

The experimental results show that the GAN-LSTM model can effectively predict the SOH of the same battery and achieve high accuracy. The error is stable within 3%, which preliminarily proves the predictive feasibility of the model.

To further verify the effectiveness of the proposed algorithm, we used the first 20%, 30% and 50% of the B0005 and B0006 sample data as the training set, and performed SOH prediction on the B0007 sample to compare the SOH under different data sets. The effect of prediction can prevent over-fitting and over-learning due to the large training set, so as to obtain the optimal solution.

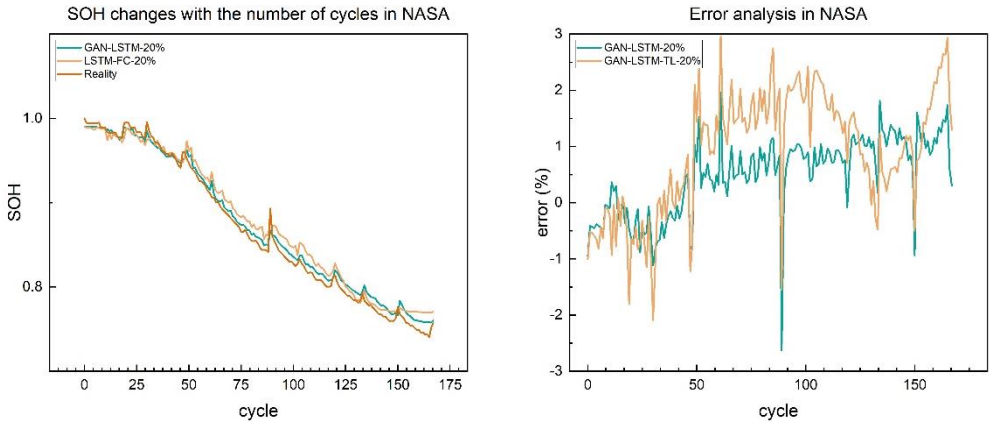

(a) SOH changes with the number of cycles (20%) (b) Error analysis (20%)

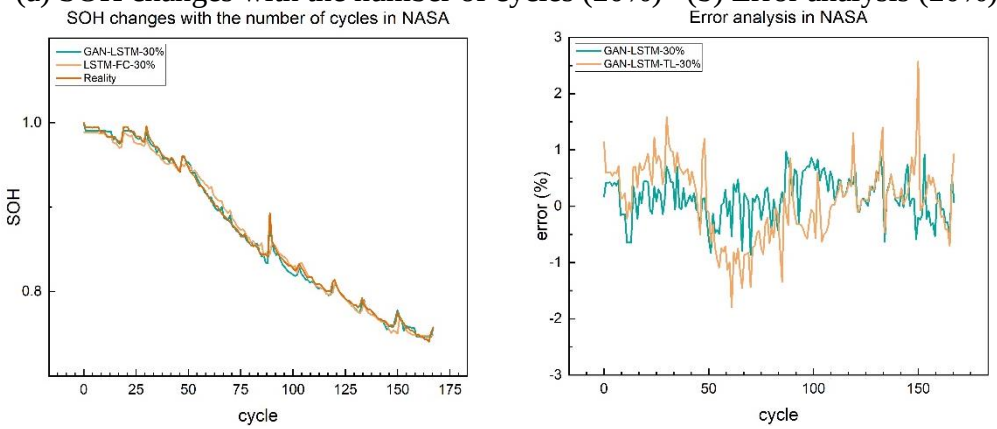

(a) SOH changes with the number of cycles (30%) (b) Error analysis (30%)

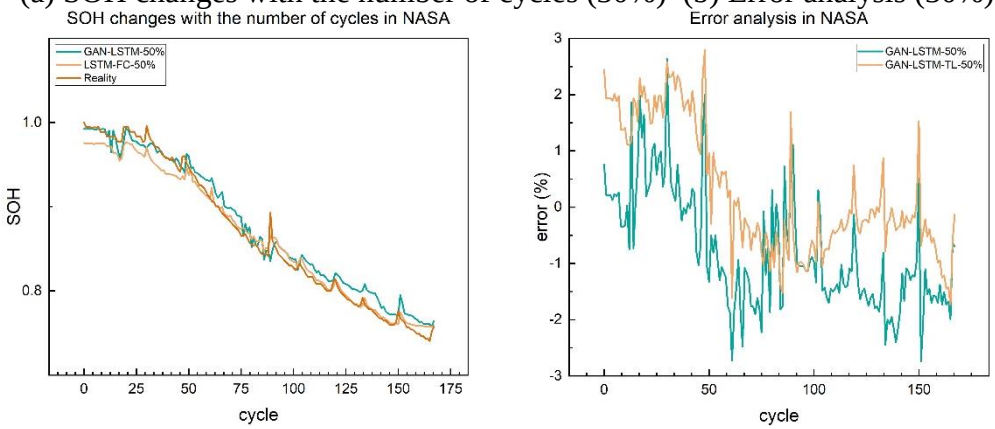

(a) SOH changes with the number of cycles (50%) (b) Error analysis (50%)

Figure 9. Performance comparison of GAN-LSTM and LSTM on B0007 dataset.

In order to verify the advanced nature of the proposed SOH prediction method, we set up multiple groups of control experiments to respectively prove the accuracy of this study. The prediction results and error curves of the model are shown in Fig. 9, and the specific error conditions are shown in Table 1.

Table 1. Performance of GAN-LSTM and LSTM on B0007 dataset

	MAE	RMSE
LSTM-FC-20%	0.1210	0.1408
GAN-LSTM-20%	0.0742	0.0853
LSTM-FC-30%	0.0561	0.0761
GAN-LSTM-30%	0.0334	0.0410
LSTM-FC-50%	0.1165	0.1966
GAN-LSTM-50%	0.0954	0.1381

It can be seen from the figure that the predicted curve is always close to the actual SOH curve throughout the prediction stage. For the division of different datasets, the prediction effect under 30% dataset is the best. For different schemes, within the SOH range allowed by the battery, the prediction accuracy of GAN-LSTM is significantly higher than that of LSTM-FC, the fitting is more accurate, and higher accuracy can be achieved in a smaller dataset. The prediction accuracy of GAN-LSTM is significantly improved compared to LSTM alone.

The prediction results of this study are consistent with the corresponding conclusions of the prediction performance analysis. Through the dual processing of GAN and data set division, the problem of accuracy decline caused by over-fitting is effectively solved, and it has good estimation accuracy and robustness. There is still a lot of space for development in processing the smaller datasets.

4.2. Performance of GAN-LSTM-TL on CALCE dataset

To verify the performance of the model transfer learning, we implemented a fine-tuning strategy for the CALCE dataset, loaded the weights of the GAN and the second LSTM recurrent neural network layer, set the front to a frozen state, and randomly initialized other dense layers. Other layers are set to trainable state. Using the top 20%, 30% and 50% of the sample data of samples CS2_35 and CS2_36 as the training set, SOH prediction is performed on the sample CS2_37. The maximum number of iterations for all CALCE datasets is 100, the sliding window size is 16, the number of samples (batch size) is 16, the number of neurons in the hidden layer is 128, the learning rate is 0.01, and the last layer is set as a fully connected layer. To enhance robustness, a Dropout layer with a value of 0.01 is set.

We have carried out several sets of control experiments to verify that the experimental results are the optimal solution. The specific error situation is shown in Table 2, and the error curve is shown in Figure 10.

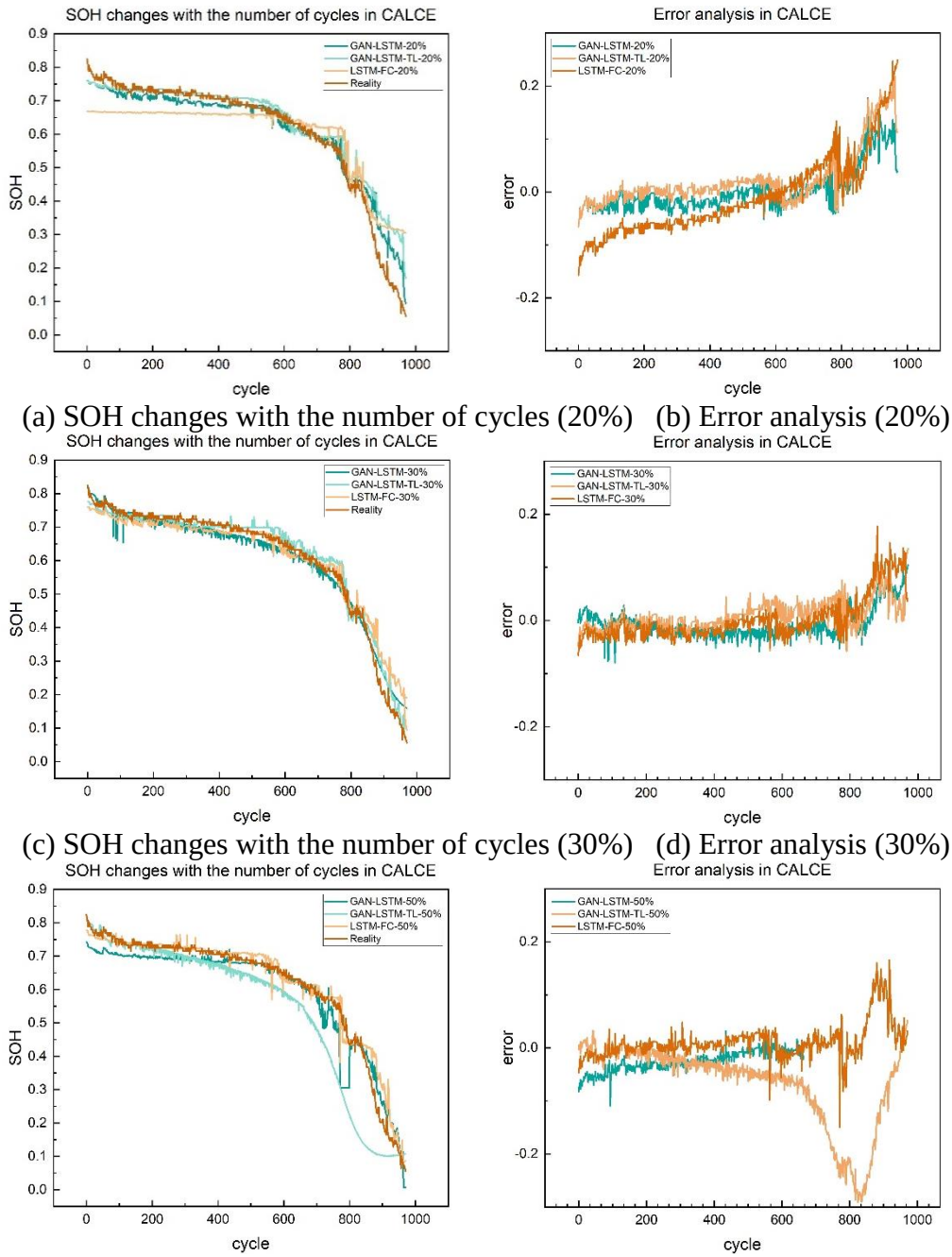

(a) SOH changes with the number of cycles (20%) (b) Error analysis (20%)

(c) SOH changes with the number of cycles (30%) (d) Error analysis (30%)

(e) SOH changes with the number of cycles (50%) (f) Error analysis (50%)

Figure 10. Performance comparison of GAN-LSTM and LSTM on CS2_37 dataset.

Two outliers with large fluctuations appear in Figure 10(f), which have been handled manually. The reason for the prediction abnormality is that the data set is too large and does not match the learning rate.

From the analysis of the experimental results, it can be seen that compared with the most basic LSTM model, the fitting effect of GAN-LSTM and GAN-LSTM-TL is better. Among them, GAN-LSTM-TL can achieve the RMSE of 0.0275 in 30% of the data set of suitable size, which is significantly lower than the most basic LSTM-FC by 29.5%, and the accuracy is also much higher than that of LSTM

in a larger data set. This verifies the effect of GAN and TL on the improvement of prediction accuracy based on the LSTM model, and further shows that transfer learning can achieve more robust prediction performance. Furthermore, with the smaller 20% dataset, the effect of transfer learning decreases, resulting in higher RMSE for GAN-LSTM-TL than for GAN-LSTM.

In addition, to verify the advancement of the proposed SOH prediction method, we compare it with other experiments also performed under the CALCE dataset, including LSTM-Sliding Window-Sparse Sampling (LSTM-LWS) [33], Stacked LSTM [34], Bi-LSTM [35], PSO-SVR [14] and results to demonstrate the accuracy of this study. The specific comparison results are shown in TABLE 3, 4 and 5.

Table 2. Performance of GAN-LSTM and LSTM on CS2_37 dataset

	MAE	RMSE
LSTM-FC-20%	0.0611	0.0765
GAN-LSTM-20%	0.0284	0.0402
GAN-LSTM-TL-20%	0.0331	0.0573
LSTM-FC-30%	0.0284	0.0390
GAN-LSTM-30%	0.0219	0.0280
GAN-LSTM-TL-30%	0.0208	0.0275
LSTM-FC-50%	0.0687	0.1034
GAN-LSTM-50%	0.0350	0.0491
GAN-LSTM-TL-50%	0.0298	0.0403

Table 3. Performance of different experiments on CS2_37 dataset

	MAE	RMSE
GAN-LSTM-TL	0.0208	0.0275
LSTM-FC	0.0284	0.0390
LSTM-LWS[33]	—	0.2106

For the CALCE dataset, MAE and RMSE were negatively correlated with prediction accuracy. As shown in TABLE 3, in comparison with the basic LSTM-FC model and the LWS model [33], the prediction curve of GAN-LSTM-TL has the smallest overall error, obtaining the smallest MAE value = 0.0208 and a smaller RMSE = 0.0275, a higher accuracy has been achieved within the allowable range of battery usage.

Table 4. Performance of different experiments on CS2_37 dataset

	MAE	RMSE
GAN-LSTM-TL	0.0208	0.0275
StackedLSTM[34]	0.0333	0.0186
Bi-LSTM[35]	0.0350	0.0261

As shown in TABLE 4, the difference between MAE and RMSE of the GAN-LSTM-TL model is smallest, and more stable prediction results can be obtained. It is worth noting that the MAE=0.0333

of the Stacked LSTM model [34] is 60.1% higher than this model; RMSE=0.0186, which is 30.7% lower than this model. The MAE of the Bi-LSTM model [35] is 0.0350, which is 68.3% higher than this model; but RMSE=0.0261, which is 5.1% lower than this model. This is because the amount of data in the application of this model is small, the curve is relatively smooth, and the fitting curve is closer to the trend of the normal curve; however, there is still room for improvement in the prediction of some special values or outliers.

Table 5. Performance of different experiments on CS2_37 dataset

	MAE	RMSE
GAN-LSTM-TL	0.0208	0.0275
PSO-SVR(30%)[14]	—	0.0287
PSO-SVR(100%)[14]	—	0.0245

As shown in TABLE 5, compared to other models based on LSTM networks, GAN-LSTM-TL can achieve higher accuracy with a smaller 30% dataset. In the case of the PSO-SVR method [14] using 100% dataset, the RMSE can reach 0.0245, but in practical applications with smaller datasets, the GAN-LSTM-TL model using 30% dataset can achieve better results and good prediction effect.

5. CONCLUSION

This thesis proposes a new method for Li-ion battery SOH prediction based on GAN-LSTM-TL network. The main contributions are as follows:

(1) GAN is used to process the corresponding feature data to generate the dataset for training;

(2) LSTM network is used to learn the dependency between feature quantity and SOH to obtain SOH estimation results;

(3) TL is used to transfer various models to the CALCE dataset in a bid to enhance the adaptability of the network model and minimize workload. To achieve the purpose of improving the generalization ability of the model, so as to accurately estimate the SOH of different battery data sets.

In a nutshell, the method proposed in this thesis is of great significance for SOH prediction of Li-ion batteries in a wide range of circumstances. Different from traditional transfer learning, the proposed SOH prediction method is able to adapt to diverse sizes and kinds of battery datasets. The downside of this method is that it must be constructed on the prediction assignment with the same charging procedure and feature quantity, which may not be applicable to several types of battery datasets. As a result, we are obliged to extract corresponding feature quantities according to the different battery datasets. In addition, the charging process of the prediction task of transfer learning is consistent with the base model, which limits the application of other charging process batteries. In the future, other transfer learning methods will be designed for different charging types of lithium batteries. Furthermore, how to create a rather more accurate and faster SOH estimate method with increased efficiency and minimal data is a topic worthy of attention in follow-up research.

CONFLICTS OF INTEREST
The authors declare there is no potential conflict of interest involved in this writing process.

ACKNOWLEDGMENTS
This work was supported by the joint fund project of the Ministry of Education of 391 China(8091B022133).

References

1. A.C. Caliwag and W. Lim, *IEEE Access*, 7(2019)59680-59689.
https://doi.org/10.1109/ACCESS.2019.2914188
2. X. Shu, J. Shen, G.Li, Y. Zhang and Y. Liu, *IEEE T Transp Electr*, 99(2021)1.
https://doi.org/10.1016/j.isci.2021.103265
3. JK. Si, SH. Kim, HM. Lee, SH. Lim and YJ. Shin, ISIE 2020, Delft, *Netherlands*, 2020, 1336-1341.
https://doi.org/10.1109/ISIE45063.2020.9152544
4. X. Hu, J. Jiang, D. Cao, and E. Bo, *IEEE T Ind Electron*, 63(2016)2645-2656.
https://doi.org/10.1109/TIE.2015.2461523
5. A. Guha and A. Patra, *IEEE T Transp Electr*, 4(2018)135-146.
https://doi.org/10.1109/TTE.2017.2776558
6. SH. Kim, HM. Lee, GY. Kwon, I. Park and YJ. Shin, ISIE 2019, Vancouver, *Bc, Canada*, 2019, 1971-1976.
http://dx.doi.org/10.1109/ISIE.2019.8781285
7. H. Pan, C. Chen, M. Gu, ENERGIES, 15(2022)1-15.
https://doi.org/10.3390/en15155686
8. X. Yang, S. Wang, W. Xu, J. Qiao, C. Yu, P. Takyi-Aninakwa and S. Jin, *Electrochim Acta*, 415(2022)140241.
https://doi.org/10.1016/j.electacta.2022.140241
9. XL. A, CY. B, ZW. C, JH. D,SY. B, *Etransportation*, 11(2022)100156.
https://doi.org/10.1016/j.etran.2022.100156
10. C. Rossi, C. Falcomer, L.Biondani and D. Pontara, *Energies*, 15(2022)3404.
https://doi.org/10.3390/en15093404
11. Y. Xu, H. Shu, H. Qin, X. Wu, J. Peng, C. Jiang, Z. Xia, Y. Wang and X. Li, *Energies*, 15(2022)2534.
https://doi.org/10.3390/en15072534
12. D. Selvabharathi and N. Muruganantham, *J Circuit Syst Comp*, 31(2022)2250081.
https://doi.org/10.1142/S0218126622500815
13. S. Jo, S. Jung and T. Roh, *Energies*, 14(2021)7206.
https://doi.org/10.3390/en14217206
14. K. Q. Zhou, Y. Qin, B. P. L. Lau, C. Yuen and S. Adams, IECON 2021, Toronto, CANADA, 2021.
https://doi.org/10.48550/arXiv.2109.13448
15. R. Li, W. Li, H. Zhang, Y. Zhou and W. Tian, *Front Energy Res*, 9(2021)693249.
https://doi.org/10.3389/fenrg.2021.693249
16. J. Zhang, J. Hou and Z. Zhang, CCDC 2020, Hefei, CHINA, 2020.
http://dx.doi.org/10.1109/ICPSAsia48933.2020.9208399
17. Q. Liu, Y. Kang, S. Qu, B. Duan and C. Zhang, I&CPS Asia 2020, Shandong, CHINA, 2020.
http://dx.doi.org/10.1109/ICPSAsia48933.2020.9208399
18. Y. Wang, X. Dong, L.Wang, W. Chen and X. Zhang, *Acm T Archit Code* OP, 19(2022)13.
https://doi.org/10.1145/3500917

19. P. Das, S. Kumar, G. Panda and D. S. Roy, *Sustainable Energy and Technological Advancements*, Springer, (2022)Singapore, Singapore.
https://doi.org/10.1007/978-981-16-9033-4_52
20. N. Javaid, H. Gul, S. Baig, F. Shehzad and T. Sultana, *IEEE Acces*, 99(2021)1-1.
https://doi.org/10.1109/ACCESS.2021.3092645
21. S. Li, H. He, P. Zhao, S. Cheng and J. Yan, *Appl Energ*, 316(2022)119120.
https://doi.org/10.1016/j.apenergy.2022.119120
22. Z. Bao, J. Jiang, C. Zhu and M. Gao, *Energies*, 15(2022)4399.
https://doi.org/10.3390/en15124399
23. F. Cadini, C. Sbarufatti, F. Cancelliere and M. Giglio, *Appl Energ*, 235(2019)661-672.
https://doi.org/10.1016/j.apenergy.2018.10.095
24. H. Wei, N. Williard, M. Osterman and M. Pecht, *J Power Sources*, 196(2011)10314-10321.
https://doi.org/10.1016/j.jpowsour.2011.08.040
25. Y. Xing, E. Ma, K. L. Tsui and M. Pecht, *Microelectron Reliab*, 53(2013) 811-820.
https://doi.org/10.1016/j.microrel.2012.12.003
26. Y. Yu, A. Srivastava and S. Canales, *ACM T Multim Comput*, 17(2021)1-20.
http://dx.doi.org/10.1145/3424116
27. A. Radford, L. Metz and S. Chintala, ICLR 2016, San Juan, Puerto Rico, 2015.
https://doi.org/10.48550/arXiv.1511.06434
28. F. A. Gers, J. Schmidhuber, F. Cummins, *Neural Comput*, 2(1999)850-855.
https://doi.org/10.1162/089976600300015015
29. D. Kingma and J. Ba, *Comput Sci*, v9(2017)arXiv:1412.6980.
https://doi.org/10.48550/arXiv.1412.6980
30. Y. Guo, H. Shi, A. Kumar, K. Grauman, T. Rosing and R. Feris, CVPR 2019, Long Beach, CA, USA, 2019.
https://doi.org/10.48550/arXiv.1811.08737
31. T. Fu, T. Zhang and X. Song, *Energies*, 15(2022)1-17.
https://doi.org/10.3390/en15082907
32. X. Shu, J. Shen, G. Li, Y Zhang and Y. Liu, *IEEE T Transp Electr*, 99(2021)1.
http://dx.doi.org/10.1109/TTE.2021.3074638
33. C. Song and S. Lee, IMCOM 2021, Seoul, Korea, 2021.
http://dx.doi.org/10.1109/IMCOM51814.2021.9377402
34. U. Yayan, A. T. Arslan and H. Yucel, *Appl Artif Intell*, 35(2021)1-19.
http://dx.doi.org/10.1080/08839514.2021.1901033
35. Y. Tan and G. Zhao, *IEEE T Ind Electron*, 67(2019)8723-8731.
http://dx.doi.org/10.1109/TIE.2019.2946551